Kovove Mater. 61 2023 351–357
DOI: 10.31577/km.2023.6.351

Effect of 5.31Ti (at.%) content used as ternary in quaternary Cu-rich high-temperature shape memory alloy cast via arc melting

Güneş Başbağ[1], Oktay Karaduman[2]*, Canan Aksu Canbay[3], İskender Özkul[4], Mustafa Boyrazlı[1]

[1] *Department of Metallurgical and Materials Engineering, Engineering Faculty, Firat University, Elazig, Turkey*
[2] *Rare Earth Elements Application and Research Center, Munzur University, Tunceli, Turkey*
[3] *Department of Physics, Faculty of Science, Firat University, Elazig, Turkey*
[4] *Department of Mechanical Engineering, Faculty of Engineering, Mersin University, Mersin, Turkey*

Received 22 December 2021, received in revised form 30 April 2023, accepted 23 June 2023

Abstract

In this work, the new quaternary CuAlTiMg high-temperature shape memory alloy (HTSMA) with an unprecedented composition and with extended solubility of Ti was produced by the arc melting method. The thermal shape memory effect characterization tests were done by performing a series of differential calorimetric (DSC and DTA) measurements. The obtained thermograms of the alloy displayed the martensitic phase transformation peaks. The forward (martensite to austenite) phase transformation was found to occur at above 350 °C, which qualifies the produced alloy as an HTSMA. The microstructural XRD measurement was performed to reveal the atomic planes of martensite structures formed in the alloy, which constitute the shape memory effect property of the fabricated alloy. The alloy surface was monitored by optical microscopy image taken at room temperature, and finely dispersed Ti-rich X-phases were observed.

K e y w o r d s: CuAlTiMg high-temperature shape memory alloy (HTSMA), shape memory effect, martensitic transformation, differential scanning calorimetry (DSC), differential thermal analysis (DTA), arc melting

1. Introduction

Varying industrial demands on the utilization of shape memory alloys (SMAs) depending on the application type have been increasing. Such demands can be either reducing the production costs of these unique and versatile smart alloys or improving their performance and modifying their properties, or else. A promising SMA group is Cu-based SMAs. Since the most commercially used NiTi-based SMAs with superior SMA properties have high costs and hard processing disadvantages, research on Cu-based SMAs (regarded as the closest alternative to NiTi SMAs) has gained importance. Doping the binary or ternary Cu-based shape memory alloys (e.g., CuAlMn, CuAlNi, CuZnAl,...) with one (quaternary) or more elements is one of the much-used methods to modify characteristic martensitic phase transformation temperatures (operation temperatures), reduce brittleness, improve ductility, enhance shape memory capacity, superelasticity, damping properties, and so forth.

High-temperature shape memory alloys (HTS--MAs) have been ever-increasingly demanded in many related high-tech industrial applications such as automotive or aerospace [1–3], too. As generally defined, an HTSMA has characteristic martensitic (operation) temperatures above $\sim 100\,°C$ (or $A_s > 390\,K$) [2, 3]. Since the most expensive but superior binary NiTi-based shape memory alloys (SMAs) have limited ($M_s < 87\,°C$) maxima transformation temperatures [3], their transformation temperatures have been elevated by additive elements such as Au, Pt, Pd, Zr, or Hf [2, 4, 5] in the last decades.

However, this recipe of alloying with such expensive additive elements also increased the aforetime costs and processing difficulties of NiTi-based

*Corresponding author: e-mail address: oktaykaraduman@munzur.edu.tr

(HT)SMAs more. Therefore, researchers have also been searching for an alternative to NiTi-based HT/SMAs by focusing on cost-effective Cu-based SMAs with ease of processing, especially CuAl-based HT/SMAs (e.g., CuAlNi or CuAlNiMn) [1–3, 6].

Ti element has been used as a grain refining and alloy strengthening element by adding minor amounts of it into the ternary Cu-based SMAs [7–9]. However, the low solubility of Ti in the Cu matrix leads to the form of Ti-rich X-phase precipitations [8]; therefore, its solid solubility and incorporation in the Cu-based alloy matrix is limited. Nevertheless, an extended solid solubility of Ti in melt-spun Cu-Ti alloy up to 7–8 wt.% (whereas by quenching up to 6 wt.%) has been demonstrated previously [10]. Therefore, using Ti content as an alloying element in some larger amounts can be possible. Previously, using 1.85 at.% of Ti in the quaternary Cu-24.07Al-1.85Ti-1.40Co (at.%) HTSMA [11] was successfully demonstrated, and the transformation temperatures of that alloy had been reported in the range of $\sim 234\,^{\circ}\mathrm{C}$ ($= M_f$) and $\sim 404\,^{\circ}\mathrm{C}$ ($= A_f$).

In this work, Ti element was used as the third (ternary) alloying element in the arc-melted quaternary CuAlTiMg HTSMA with an alloy composition of 71.89Cu-22.53Al-5.31Ti-0.26Mg (at.%). The characteristic transformation temperatures, shape memory effect, and the related microstructural properties of the alloy were investigated by thermal and structural measurements in detail.

2. Experimental

In this work, the quaternary CuAlTiMg alloy with unprecedented alloy composition of 71.89Cu-22.53Al-5.31Ti-0.26Mg (at.%) was produced by mixing the powders of high purity (99.9 %) elements of Cu, Al, Ti, and Mg elements. The powder mixture was pelletized under pressure, and then the obtained pellets were all together melted in an arc melter under an argon plasma atmosphere, and the alloy was obtained as-cast ingot. Then the ingot alloy was cut into small slab samples ($\sim 4 \times 4 \times 2.5\,\mathrm{mm}^3$ and ~ 25–$55\,\mathrm{mg}$), and these samples were together heat-treated (homogenized) at 900 °C for 1 h and immediately were all quenched in iced-brine water environment by which the martensite structure was formed in the alloy to have a shape memory effect. The differential scanning calorimetry (DSC) tests were carried out by using a Shimadzu 60A label DSC instrument at different 15, 25, 35, and 45 °C min^{-1} of heating/cooling rates under an inert argon gas flow of 100 ml min^{-1}. To reveal the high-temperature behavior of the alloy, the differential thermal analysis (DTA) test was taken under the same gas flow and at a single 25 °C min^{-1} heating/cooling rate between room temperature and 900 °C by using a Shimadzu DTG-60AH instrument. A Zeiss Evo MA10 model EDS (energy dispersive X-ray spectrum) instrument was used to detect the alloy composition under room conditions. The EDS result of the alloy is given in Fig. 1, and the detected alloy composition is presented in Table 1. The existence of the formed martensite structures in the alloy was demonstrated by an X-ray diffraction (XRD) test performed at room temperature by using a Rigaku RadB-DMAX II diffractometer with CuKα radiation. The optical micrograph (metallograph) displaying the alloy surface was taken at room temperature via using an optical microscope with model no. XJP-6A. Plus, an SEM image of a fractured surface of the alloy was also taken.

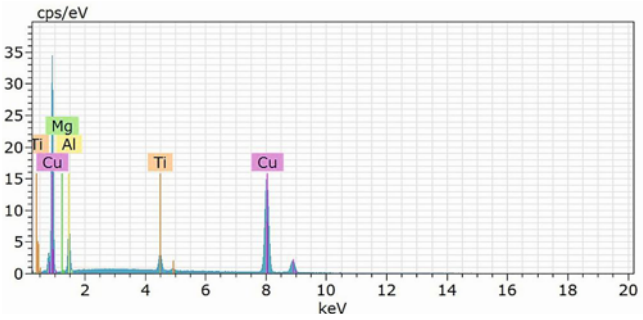

Fig. 1. The EDS spectra of the CuAlTiMg alloy.

Table 1. The detected chemical composition of the CuAlTiMg alloy

Element	(wt.%)	(at.%)	Error (wt.%)
Cu	84.02	71.89	2.07
Al	11.18	22.53	0.52
Ti	4.68	5.31	0.15
Mg	0.12	0.26	0.04

3. Results and discussion

The DSC curves of the CuAlTiMg alloy taken at different heating/cooling rates are presented in Fig. 2. According to these curves, except not clearly seen on the curves taken at 15 and 45 °C min^{-1} of heating/cooling rates, the forward downside endothermic reverse martensitic transformation (from martensite to austenite phase; M $\rightarrow$ A) peaks on the downside heating parts of these curves can be seen, and vice versa the correspondent exothermic upward A $\rightarrow$ M (direct) transformation peaks on the cooling parts of these curves [6, 9, 11–16]. On the curve taken at the rate of 45 °C min^{-1}, there occurred a temperature (thermal) lag event due to the high heating/cooling rate [17], which caused a shallowed M $\rightarrow$ A peak on

Table 2. Thermodynamical transformation temperatures and kinetic parameters of the CuAlTiMg HTSMA

Thermal test instrument	Heating/ cooling rate (℃ min^{-1})	A_s (℃)	A_f (℃)	A_{max} (℃)	M_s (℃)	M_f (℃)	A_s–M_f (℃)	T_0 (℃)	$\Delta H_{M\to A}$ (J g^{-1})	$\Delta S_{M\to A}$ (J g^{-1} ℃$^{-1}$)
DSC	15	350.62	396.12	403.84	335.63	318.73	31.89	365.87	5.25	0.01435
DSC	25	358.26	380.28	369.99	307.23	288.38	69.88	343.75	18.51	0.05385
DSC	35	363.42	387.49	374.79	309.23	276.20	87.22	348.36	16.47	0.04728
DSC	45	324.85	403.85	380.05	–	–	–	–	12.19	–
DTA	25	342.85	419.39	387.88	271.39	219.59	123.26	345.39	8.52	0.02467
	Avg.	348.00	397.43	383.31	305.87	275.73	78.06	350.84	12.19	0.03503

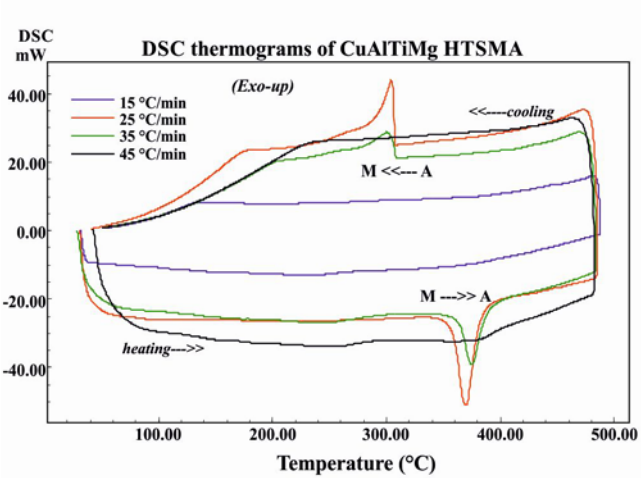

Fig. 2. The DSC curves of the CuAlTiMg high-temperature shape memory alloy.

heating and a complete disappearing of A → M peak on cooling back. The DSC measurements were taken in the order of first at 25, then at 35, 45, and lastly at 15 ℃ min^{-1} of heating/cooling rates. At the slow rate of 15 ℃ min^{-1}, taken as the last cycle, both this slow rate and the precipitations that might have formed in the proximity of the alloy's eutectoid region (500 ℃) may be caused to hinder this A → M transformation. But, maybe a better explanation of the main reason for the shallowing or disappearing of these martensitic transformation peaks (especially those seen at the rate of 15 ℃ min^{-1}) will be given by the discussion made upon the XRD pattern and optical microscopy image of the alloy ahead.

The martensitic transformation temperatures (A_s, A_f, M_s, M_f, and also A_{max}), hysteresis gap (A_s–M_f) values, enthalpy change ($\Delta H_{M\to A}$), and some other important thermodynamical parameters obtained by applying DSC tangent peak analyses on these peaks and by calculations made upon these analyses data are all presented in Table 2. As seen in this table, the transformation temperatures are all far above 100 ℃ (in general $A_s > \sim 350$ ℃), which ascribes the produced CuAlTiMg alloy that it is a high-temperature shape memory alloy, and the large enthalpy change values indicate the powerful shape memory effect property of the alloy.

In Table 2, the values of the thermal equilibrium temperature (T_0), i.e., where is no difference between the Gibbs (chemical) free energies of martensite and austenite phases, were found by using $T_0 = 0.5(A_f + M_s)$ formula [17]. The amounts of the entropy change, ΔS, that occurred during M → A transformations were determined by using $\Delta S_{M\to A} = \Delta H_{M\to A}/T_0$ formula [13, 14].

There is another important reaction kinetic parameter of SMAs that determines the nature of the crystallization behavior of the SMAs, the activation energy (E_a) parameter, which is the energy needed for a martensitic transformation to occur. The E_a value of the CuAlTiMg HTSMA was computed by using the Kissinger formula [13] given below:

$$\mathrm{d}\left[\ln \Phi/T_m^2\right]/\mathrm{d}\left(1/T_m\right) = -E_a/R, \qquad (1)$$

where Φ is the heating/cooling rate, T_m is the maximum temperature (A_{max}) of M → A transformation peak, and R is the universal gas constant ($R = 8.314$ J mol^{-1} K^{-1}). The term on the left side of this equation is equal to the linear fitting slope of the plot of d[ln Φ/T_m^2] versus $1000/T_m$ that was drawn (without involving the values obtained at 15 ℃ min^{-1} of DSC heating rate) and given in Fig. 3. This plot depictures change in the activation energy depending by heating rate. By substituting the slope value instead of the left term in Eq. (1), the E_a value of the alloy was found as 192.82 kJ mol^{-1}.

The DTA curve of the produced CuAlTiMg HTSMA taken at a single 25 ℃ min^{-1} of heating/cooling rate is given in Fig. 4. The multiple peaks that emerged back-to-back on this DTA curve indicate the common high-temperature behavior pattern of Cu-based SMAs [9, 11, 13–16, 20–26] and this behavior consisting of successive multistage phase transitions on heating and vice versa on cooling a Cu-based SMA is like this: $\beta1'$(with $\gamma1'$) → $\beta1(L2_1)$ →

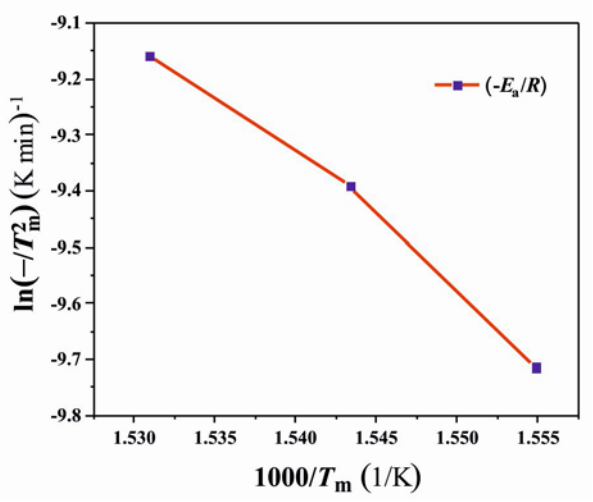

Fig. 3. The plot of the change in the E_a activation energy of the CuAlTiMg HTSMA.

meta-$\beta 2$(B2) $\rightarrow \alpha + \gamma 2$ (precipitations) $\rightarrow$ eutectoid reaction $\rightarrow \beta 2$(B2, ordered) $\rightarrow$ A2(disordered).

The average conduction (or valence) electron concentration (e/a ratio) is an important parameter for Cu-based SMAs to have a shape memory effect (SME) property, and a theoretical forecast can be made upon the presence of the formed martensite structures and their volumetric dominance over each other in a Cu-based SMA by determining the value of its e/a ratio [13, 14, 18, 19]. The Cu-based SMAs generally have an SME property at their e/a values in between the range of 1.45–1.49; for the e/a values in between this range the monoclinic $\beta 1'$(M18R) and the hexagonal $\gamma 1'$(2H) types of martensite structures will form nearly in equal volumes, below this e/a range the M18R martensite will have a larger volume than 2H martensite will do, and above this range at this time the 2H martensite forms will gain dominancy over the M18R martensite forms [13, 14, 20]. The e/a ratio of the CuAlTiMg HTSMA was calculated as 1.506 by using $e/a = \sum f_i v_i$ formula [13, 14, 21], where f_i refers to the atomic fractions (at.%) of the alloying elements and v_i is the valence electron numbers of these elements. Therefore, the e/a value of 1.506 implies that the produced CuAlTiMg HTSMA contains both $\beta 1'$(18R) and $\gamma 1'$(2H) types of martensite structures that coexistently formed nearly in equal volumes, which is shown by the following structural X-ray diffraction pattern of the alloy as below.

The XRD pattern of the CuAlTiMg HTSMA obtained at room temperature is presented in Fig. 5. The highest peak on this pattern is the $\beta 1'(0018)$ peak of the M18R($\beta 1'$) type martensite phase, and the other peaks are (0018), (128), (1210), (2012), (2010), (040), (042) and (320) peaks of $\beta 1'$ martensite, a $\gamma 1'(002)$ and an X-Ti(400) precipitation (X-phase; Ti3.3Al) peak with low intensity [7, 11, 22, 27]. As it is seen, the high-intensity peaks of $\beta 1'(0018)$ and $\gamma 1'(002)$ confirm the coexistence of these martensite phases [27]. The low-intensity Ti-rich X-phase precipitation peak signifies that at room temperature, some of the 5.31Ti (at.%) content in the Cu-based alloy matrix has not dispersed in the alloy and precipitated, but the solubility of Ti might have decreased by the effect of the thermocyclic heating/cooling test processes (of DSC and DTA), alike by the effect of annealing [28], that could cause some diffusion or

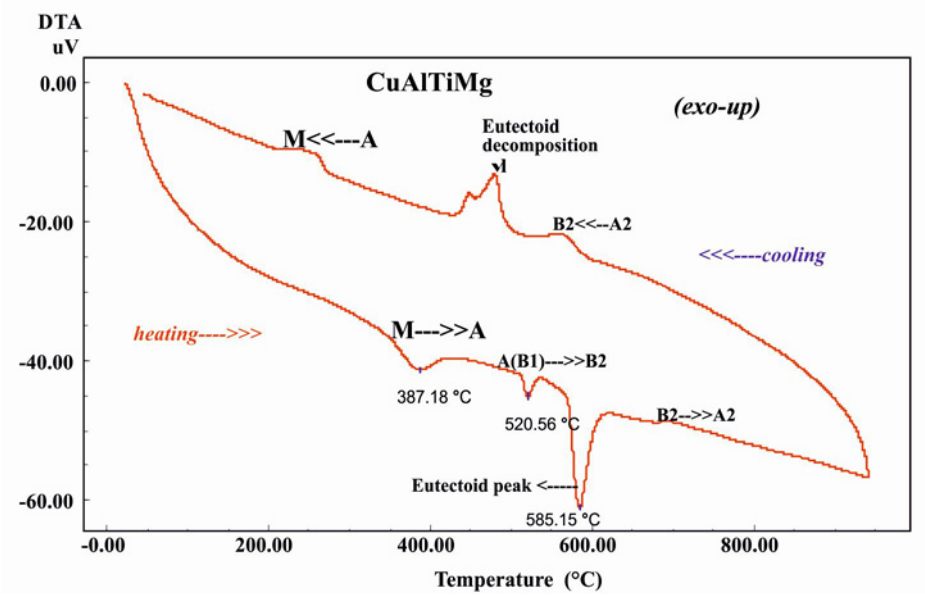

Fig. 4. The cyclic DTA curve of the CuAlTiMg HTSMA taken at a single 25 °C min^{-1} of heating/cooling rate.

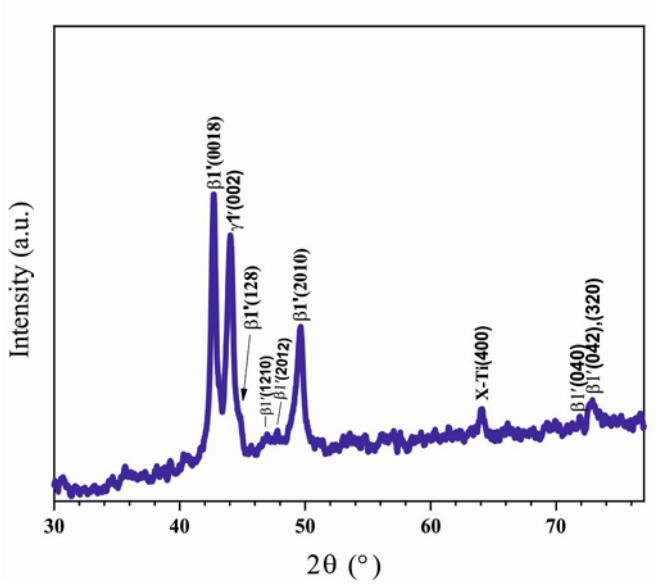

Fig. 5. The XRD pattern of the CuAlTiMg HTSMA obtained at room temperature.

disassociation of Ti atoms apart from their initial solute positions in the Cu-based alloy lattice leading to form more X-precipitations and thus hinder the martensitic transformation as mentioned in the above discussions made on the DSC results of the alloy. On the other hand, in the previous work [7], it was stated that a complete disappearance of the X-phase peak stemmed from a low density of X-phases in the microstructure that resulted from an increment of Ti (up to 1 wt.%) content. Therefore, it can be said that even if some of the Ti content is precipitated at room temperature, the solubility limit of Ti and stability of martensitic transformation (in this novel CuAlTiMg alloy) will be high if the alloy's temperature is only changed in between transformation (working) temperatures region (between at around M_f and A_f temperatures) of the alloy without reaching too far up (to metastable B2 phase region and/or hypoeutectoid temperature region) or too far down (to room temperature).

The average crystallite size (D) of the CuAlTiMg HTSMA was calculated by using the Debye-Scherrer formula [13, 29] as given below:

$$D = \frac{0.9\lambda}{B_{1/2}\cos\theta}, \tag{2}$$

where λ refers to the X-ray wavelength of the CuKα radiation ($\lambda = 0.15406$ nm), and $B_{1/2}$ refers to the full width at half maximum (FWHM) value of the highest intensity peak (the FWMH value is 0.369 at $2\theta = 42.681°$). The average crystallite size value of the CuAlTiMg HTSMA was found as 23.12 nm [7, 11].

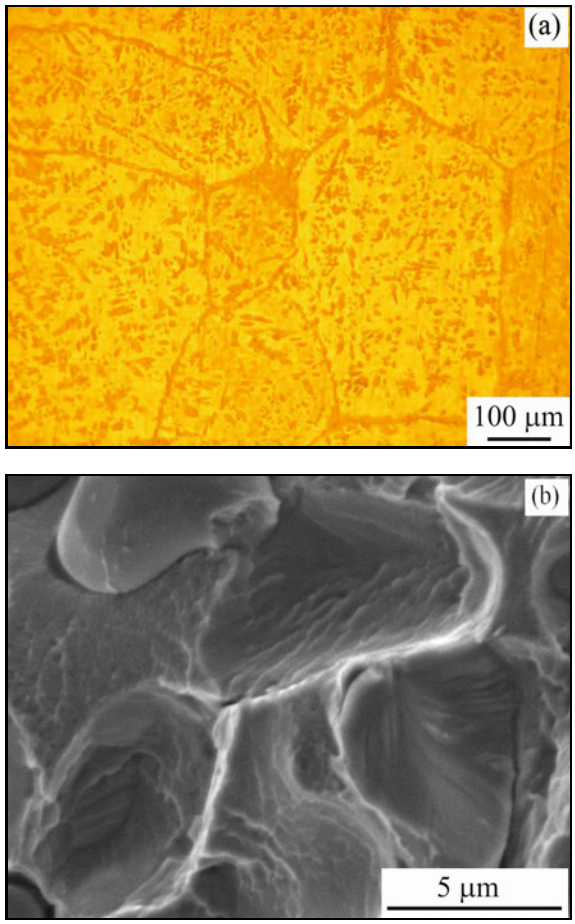

Fig. 6. (a) The optical microscopy image of the CuAlTiMg HTSMA obtained at room temperature wherein the grains and grain borders of the alloy can be clearly seen in this image, (b) the SEM image of a fractured surface of the alloy.

The optical microscopy image (metallograph) of the produced alloy is presented in Fig. 6a. As seen in this image here, the grain boundaries between the surface grains of the alloy can be clearly seen. The image was taken at room temperature (far below the alloy's average M_f temperature of 275.73 ℃) where the alloy is in the martensite phase; therefore, the solubility of Ti enormously decreased in the Cu-rich matrix at room temperature [30], and this causes the formation of intermetallic compounds or Ti-rich (or Ti-borne) X-phases precipitations which lead changes in the composition of the austenite phase of the alloy [30, 31]. These X-phases (seen as finely dispersed dark spots in this metallograph) reduce the mobility of interfaces between the martensite and β-phase, barricade to grain boundary migration, refine the grain size and raise the transformation temperatures [7, 18, 27, 30–33]. Apart from a thermal lag event occurring at high DSC heating/cooling rates, the compositional changes depending on the solubility of Ti changing

by temperature and formation of these size- or type-variable intermetallic/precipitation phases is the main reason for the changes (shallowing or disappearing) seen in between the martensitic transformation peaks of the alloy appeared on the DSC curves taken at different heating/cooling rates. There is also an SEM image of a fractured surface of the alloy given in Fig. 6b, which image was taken after the end of one and a half years of the aging time of the alloy left in room conditions.

4. Conclusions

The CuAlTiMg high-temperature shape memory alloy was successfully produced by the arc melting method. The characteristic transformation temperatures of the alloy were found averagely between 275–400 °C, where A_s temperatures were generally above 350 °C. The high enthalpy changes that occurred during thermally induced martensitic transformations were found to be high, indicating the powerful shape memory effect of the alloy. The use of ternary 5.31Ti (at.%) content in the quaternary CuAlTiMg alloy resulted in high transformation temperatures but also led to the formation of some Ti-rich X-phases that were observed as a low-intensity peak in the XRD result of the produced HTSMA, and this low-intensity peak indicates the high solid solubility of Ti element in the alloy that decreases during heating (DSC, DTA) or annealing processes. In the use of the newly produced HTSMA, to prevent compositional changes and related phase transitional instabilities, the alloy's temperature should be changed around its transformation (working) temperatures. In conclusion, the produced CuAlTiMg HTSMA may be useful in HTSMA-related research and applications such as automotive or aerospace.

Acknowledgement

This research work is a part of the Ph.D. thesis works of Güneş Başbağ at Firat University, Faculty of Engineering, Department of Metallurgy and Materials Engineering.

References

[1] J. M. Jani, M. Leary, A. Subic, M. A. Gibson, A review of shape memory alloy research, applications and opportunities, Materials Design (1980–2015) 56 (2014) 1078–1113. https://doi.org/10.1016/j.matdes.2013.11.084

[2] J. Ma, I. Karaman, R. D. Noebe, High temperature shape memory alloys, International Materials Reviews 55 (2010) 257–315. https://doi.org/10.1179/095066010X12646898728363

[3] I. López-Ferreño, J. F. Gómez-Cortés, T. Breczewski, I. Ruiz-Larrea, M. L. Nó, J. M. San Juan, High-temperature shape memory alloys based on the Cu-Al-Ni system: design and thermomechanical characterization, Journal of Materials Research and Technology 9 (2020) 9972–9984. https://doi.org/10.1016/j.jmrt.2020.07.002

[4] S. Miyazaki, H. Kim, Y. Takeda, M. Tomozawa, B. Pio, High temperature shape memory alloy, actuator and motor, U.S. Patent (2009) Application No. 12/235,528.

[5] N. A. Ley, R. W. Wheeler, O. Benafan, M. L. Young, Characterization of thermomechanically processed high-temperature Ni-lean NiTi–20 at.% Hf shape memory wires, Shape Memory and Superelasticity 5 (2019) 476–485. https://doi.org/10.1007/s40830-019-00254-1

[6] Y. Gao, M. Zhu, J. K. L. Lai, Microstructure characterization and effect of thermal cycling and ageing on vanadium-doped Cu–Al–Ni–Mn high-temperature shape memory alloy, Journal of Materials Science 33 (1998) 3579–3584. https://doi.org/10.1023/A:1004647127294

[7] S. N. Saud, E. Hamzah, T. Abubakar, M. Zamri, M. Tanemura, Influence of Ti additions on the martensitic phase transformation and mechanical properties of Cu–Al–Ni shape memory alloys, Journal of Thermal Analysis and Calorimetry 118 (2014) 111–122. https://doi.org/10.1007/s10973-014-3953-6

[8] Y. C. Wee, T. A. A. Bakar, E. H. S. N. Saud, Study of X-phase formation on Cu-Al-Ni shape memory alloys with Ti addition, Journal of Mechanical Engineering and Sciences 11 (2017) 2770. https://doi.org/10.15282/jmes.11.2.2017.17.0251

[9] C. A. Canbay, M. A. Çiçek, O. Karaduman, İ. Özkul, M. Şekerci, Investigation of thermoelastic martensitic transformations and structure in the new composition of CuAlMnTi shape memory alloy, Journal of Materials and Electronic Devices 1 (2019) 60–64.

[10] S. I. Kondo, H. Nakashima, T. Morimura, On the solid solubility extension by rapid quenching and spinodal decomposition during aging in melt-spun Cu–Ti alloys, Materials Transactions 60 (2019) 338–345. https://doi.org/10.2320/matertrans.M2018255

[11] O. Karaduman, I. Özkul, S. Altin, E. Altin, Ö. Bağlayan, C. A. Canbay, New Cu-Al based quaternary and quinary high temperature shape memory alloy composition systems. AIP Conference Proceedings 2042 (2018) p. 020030. https://doi.org/10.1063/1.5078902

[12] S. Niedbalski, A. Durán, M. Walczak, J. A. Ramos-Grez, Laser-assisted synthesis of Cu-Al-Ni shape memory alloys: Effect of inert gas pressure and Ni content, Materials 12 (2019) 794. https://doi.org/10.3390/ma12050794

[13] C. A. Canbay, O. Karaduman, N. Ünlü, S. A. Baiz, I. Ozkul, Heat treatment and quenching media effects on the thermodynamical, thermoelastical and structural characteristics of a new Cu-based quaternary shape memory alloy, Composites Part B Engineering 174 (2019) 106940. https://doi.org/10.1016/j.compositesb.2019.106940

[14] C. A. Canbay, O. Karaduman, The photo response properties of shape memory alloy thin film based photodiode, Journal of Molecular Structure 1235 (2021)

130263.
https://doi.org/10.1016/j.molstruc.2021.130263
[15] S. M. Chentouf, M. Bouabdallah, J. C. Gachon, E. Patoor, A. Sari, Microstructural and thermodynamic study of hypoeutectoidal Cu–Al–Ni shape memory alloys, Journal of Alloys and Compounds 470 (2009) 507–514.
https://doi.org/10.1016/j.jallcom.2008.03.009
[16] O. Karaduman, C. A. Canbay, İ. Özkul, S. A. Baiz, N. Ünlü, Production and characterization of ternary Heusler shape memory alloy with a new composition, Journal of Materials and Electronic Devices 1 (2019) 16–19.
[17] C. A. Canbay, O. Karaduman, İ. Özkul, Lagging temperature problem in DTA/DSC measurement on investigation of NiTi SMA, Journal of Materials Science: Materials in Electronics 31 (2020) 13284–13291.
https://doi.org/10.1007/s10854-020-03881-y
[18] K. Otsuka, C. Wayman, Shape Memory Materials, Cambridge University Press, Cambridge, 1998.
[19] M. Ahlers, Phase stability of martensitic structures, Le Journal de Physique IV 5 (1995) 71–80.
https://doi.org/10.1051/jp4:1995808
[20] M. O. Prado, P. M. Decorte, F. Lovey, Martensitic transformation in Cu-Mn-Al alloys, Scripta Metallurgica et Materialia 33 (1995) 877–883.
https://doi.org/10.1016/0956-716X(95)00292-4
[21] S. M. Chentouf, M. Bouabdallah, H. Cheniti, A. Eberhardt, E. Patoor, A. Sari, Ageing study of Cu–Al–Be hypoeutectoid shape memory alloy, Materials Characterization 61 (2010) 1187–1193.
https://doi.org/10.1016/j.matchar.2010.07.009
[22] O. Karaduman, C. A. Canbay, Investigation of CuAlNi shape memory alloy doped with graphene, Journal of Materials and Electronic Devices 3 (2021) 8–14.
[23] O. Karaduman, C. A. Canbay, N. Ünlü, İ. Özkul, Analysis of a newly composed Cu-Al-Mn SMA showing acute SME characteristics, AIP Conference Proceedings 2178 (2019) 030039.
https://doi.org/10.1063/1.5135437
[24] O. Karaduman, N. Ünlü, C. A. Canbay, İ. Özkul, S. A. Baiz, The Investigation of SME in a Cu-Al-Ni HTSMA, Journal of Materials and Electronic Devices 1 (2019) 6–10.
[25] C. A. Canbay, O. Karaduman, N. Ünlü, İ. Özkul, An exploratory research of calorimetric and structural shape memory effect characteristics of Cu–Al–Sn alloy, Physica B: Condensed Matter 580 (2020) 411932.
https://doi.org/10.1016/j.physb.2019.411932
[26] O. Karaduman, C. A. Canbay, N. Ünlü, İ. Özkul, Structural and thermodynamical study of Cu-Zn-Al shape memory alloys with new compositions produced by hot isostatic press (HIP), AIP Conference Proceedings 2178 (2019) 030040.
https://doi.org/10.1063/1.5135438
[27] S. N. Saud, E. Hamzah, T. Abubakar, H. R. Bakhsheshi-Rad, R. Hosseinian, X-phase precipitation in aging of Cu–Al–Ni–xTi shape memory alloys and its influence on phase transition behavior, Journal of Thermal Analysis and Calorimetry 123 (2016) 377–389.
https://doi.org/10.1007/s10973-015-4894-4
[28] S. Tsukimoto, T. Kabe, K. Ito, M. Murakami, Effect of annealing ambient on the self-formation mechanism of diffusion barrier layers used in Cu (Ti) interconnects, Journal of Electronic Materials 36 (2007) 258–265. https://doi.org/10.1007/s11664-007-0094-8
[29] A. L. Patterson, The Scherrer formula for X-ray particle size determination, Physical Review 56 (1939) 978–982. https://doi.org/10.1103/PhysRev.56.978
[30] U. S. Mallik, V. Sampath, Influence of quaternary alloying additions on transformation temperatures and shape memory properties of Cu–Al–Mn shape memory alloy, Journal of Alloys and Compounds 469 (2009) 156–163.
https://doi.org/10.1016/j.jallcom.2008.01.128
[31] C. A. Canbay, Z. K. Genc, M. Sekerci, Thermal and structural characterization of Cu–Al–Mn–X (Ti, Ni) shape memory alloys. Appl. Phys. A 115 (2014) 371–377. https://doi.org/10.1007/s00339-014-8383-6
[32] S. N. S. Al-Humairi, Cu-based shape memory alloys: Modified structures and their related properties. In: U. B. Al-Naib, D. Vikraman and K. Karuppasamy (Eds.), Recent Advancements in the Metallurgical Engineering and Electrodeposition, IntechOpen, London, 2019, p. 25. http://dx.doi.org/10.5772/intechopen.86193
[33] J. Tian, W. Zhu, Q. Wei, S. Wen, S. Li, B. Song, Y. Shi, Process optimization, microstructures and mechanical properties of a Cu-based shape memory alloy fabricated by selective laser melting, Journal of Alloys and Compounds 785 (2019) 754–764.
https://doi.org/10.1016/j.jallcom.2019.01.153